Eur Biophys J (2013) 42:503–519
DOI 10.1007/s00249-013-0899-8

ORIGINAL PAPER

EBSA
Biophysics in Europe

^{23}Na multiple quantum filtered NMR characterisation of Na^+ binding and dynamics in animal cells: a comparative study and effect of Na^+/Li^+ competition

Carla P. Fonseca · Luís L. Fonseca · Liliana P. Montezinho · Paula M. Alves · Helena Santos · M. Margarida C. A. Castro · Carlos F. G. C. Geraldes

Received: 14 January 2013 / Revised: 7 March 2013 / Accepted: 21 March 2013 / Published online: 6 April 2013

Abstract Double quantum and triple quantum filtered ^{23}Na nuclear magnetic resonance techniques were used to characterise in detail the isotropic and anisotropic binding and dynamics of intra- and extracellular Na^+ in different cellular systems, in the absence and presence of Li^+. The kinetics of Li^+ influx by different cell types was evaluated. At steady state, astrocytes accumulated more Li^+ than red blood cells (RBCs), while a higher intracellular Li^+ concentration was found in chromaffin than in SH-SY5Y cells. Anisotropic and isotropic motions were detected for extracellular Na^+ in all cellular systems studied. Isotropic intracellular Na^+ motions were observed in all types of cells, while anisotropic Na^+ motions in the intracellular compartment were only detected in RBCs. ^{23}Na triple quantum signal efficiency for intracellular Na^+ was SH-SY5Y > chromaffin > RBCs, while the reverse order was observed for the extracellular ions. ^{23}Na double quantum signal efficiency for intracellular Na^+ was non-zero only in RBCs, and for extracellular Na^+ the order RBCs > chromaffin > SH-SY5Y cells was observed. Li^+ loading generally decreased intracellular Na^+ isotropic movements in the cells, except for astrocytes incubated with a low Li^+ concentration and increased anisotropic intracellular Na^+ movements in RBCs. Li^+ effects on the extracellular signals were more complex, reflecting Li^+/Na^+ competition for isotropic and anisotropic binding sites at the extracellular surface of cell membranes and also at the surface of the gel used for cell immobilisation. These results are relevant and contribute to the interpretation of the in vivo pharmacokinetics and sites of Li^+ action.

Keywords Multiple quantum filtered ^{23}Na NMR · Human red blood cells · Bovine chromaffin cells · Human neuroblastoma SH-SY5Y cells · Rat neurons · Rat astrocytes · Lithium

Abbreviations

α	Ratio of volume of intracellular water accessible to Li^+ ions to cell volume
A	Amplitude of the T_{31} signals
$(A_i)_t$, $(A_e)_t$ and $(A_i)_\infty$, $(A_e)_\infty$	Areas of the intra- and extracellular $^7Li^+$ NMR signals at the different times t and when the intracellular Li^+ concentration has reached a steady state, respectively
B	Amplitude of the T_{21} signals
BME	Eagle's basal medium
BMG	Basement membrane gel
C_T	Cytocrit

Electronic supplementary material The online version of this article (doi:10.1007/s00249-013-0899-8) contains supplementary material, which is available to authorized users.

C. P. Fonseca
Health Sciences Research Centre, University of Beira Interior, 6200-506 Covilhã, Portugal

L. L. Fonseca · P. M. Alves · H. Santos
Instituto de Tecnologia Química e Biológica (ITQB), Lisbon New University, Apartado 127, 2780-156 Oeiras, Portugal

L. P. Montezinho · M. M. C. A. Castro · C. F. G. C. Geraldes (✉)
Department of Life Sciences, Faculty of Science and Technology, Center for Neuroscience and Cell Biology and Coimbra Chemistry Center, University of Coimbra, P.O. Box 3046, 3001-401 Coimbra, Portugal
e-mail: geraldes@ci.uc.pt

δ	Evolution time
DMEM	Dulbecco's modified Eagle's medium
DMEM/F-12	Dulbecco's modified Eagle's medium/Ham's nutrient mixture F-12
DQF	Double quantum filtered
FBS	Fetal bovine serum
HEPES	*N*-2-hydroxyethylpiperazine-*N*′-2-ethanesulfonic acid
Ht	Hematocrit
I_{max}	Maximum intensity of the MQF
k_i	Li^+ influx rate constant
k_{iapp}	Apparent Li^+ influx rate constant
$[Li^+]_{eT}$	Total extracellular Li^+ concentration
$[Li^+]_i$	Intracellular Li^+ concentration
$[Li^+]_{if}$	Free, NMR visible, intracellular Li^+ concentration
$[Li^+]_{iT}$	Total intracellular Li^+ concentration
MQF	Multiple quantum filtered
$[Na^+]_i$	Intracellular Na^+ concentration
o.d.	Outer diameter
RBCs	Red blood cells
SQ	Single quantum
SR	Shift reagent
τ	Multiple quantum creation or preparation time
T_{2f}	Fast components of the biexponential T_2 relaxation time
T_{2s}	Slow component of the biexponential T_2 relaxation time
TQF	Triple quantum filtered
$\overline{\omega}_Q$	Residual quadrupolar coupling constant

Introduction

^{23}Na NMR is a quite useful technique for biological studies, as it uses the second strongest of all resonances in biology (Springer 1987), despite the fact that part of it is often not detectable in conventional spectra because of quadrupolar effects. It is well known that quadrupolar nuclei with spin $I = 3/2$, such as ^{23}Na, ^{39}K and ^{87}Rb, may exhibit biexponential relaxation because of their interaction with electrostatic sites on ordered biopolymers (Jaccard et al. 1986; Pekar and Leigh 1986) in systems where they rapidly exchange between free and motionally bound states. The biexponential decay of the transverse magnetisation occurs when the $-3/2 \leftrightarrow -1/2$ and $+1/2 \leftrightarrow +3/2$ outer transitions of the $I = 3/2$ nuclei relax faster than the $-1/2 \rightarrow +1/2$ inner transition (Hubbard 1970). In principle, the isolated, quadrupolar $I = 3/2$ nucleus can undergo single, double and triple quantum NMR transitions. When the nucleus-bound state is not at the extreme narrowing motional limit and undergoes biexponential relaxation, both double quantum filtered (DQF) and triple quantum filtered (TQF) NMR signals can be observed (Jaccard et al. 1986; Pekar and Leigh 1986).

Multiple quantum filtered (MQF) NMR spectroscopy has been successfully applied to quadrupolar nuclei (spin $I = 3/2$) in biological systems, in particular to characterise isotropic and anisotropic motions of bound Na^+ (Kemp-Harper et al. 1997). In isotropic systems, biexponential relaxation only leads to the creation of the third-rank tensor T_{31} because of the degeneration of the outer transitions. Thus, in this case, the DQF and TQF spectra are identical except for a 50 % increased efficiency of the TQF coherence formation (Chung and Wimperis 1990), and the respective signals consist of a positive T_{31} signal with a line shape resulting from two Lorenzian lines in antiphase. In ordered or partially ordered systems (where the average quadrupolar interaction, given by the residual quadrupolar coupling constant, $\overline{\omega}_Q$, is nonzero), the degeneracy of the outer spin transitions is lifted and the second-rank tensor T_{21} can be formed (Jaccard et al. 1986). This is detected in the DQF spectra as a broad negative component presenting a pair of overlapping dispersive lines of the satellites in antiphase, split by 2 $\overline{\omega}_Q$ (Shinar et al. 1993). Thus, ^{23}Na DQF NMR enables the detection of anisotropic motion of Na^+ because of their interaction with ordered structures in biological tissues (Eliav et al. 1992; Kemp-Harper et al. 1997). While the negative T_{21} signal is not observable in TQF spectra, a DQF spectrum that is different from the TQF spectrum is indicative of order in the biological system.

Isotropic and anisotropic motion of Na^+ was detected using this method (Kemp-Harper et al. 1997) in a variety of biological systems, in vitro and in vivo, such as animal and human tissues—cartilage, tendon, skin and spinal discs (Borthakur et al. 2002; Duvvuri et al. 1998; Eliav and Navon 1994; Eliav et al. 1992; Insko et al. 1999; Ooms et al. 2008a, b; Reddy et al. 1997; Shinar et al. 1995), organs—salivary glands, breast, muscle, heart, liver and brain (Dizon et al. 1996; Duvvuri et al. 1999; Hutchison et al. 1993; Insko et al. 1999; Jelicks and Gupta 1993;

Kalyanapuram et al. 1998; Kemp-Harper et al. 1994; Kushnir et al. 1997; Lyon and McLaughlin 1994; Lyon et al. 1991; Navon et al. 1994; Payne et al. 1990; Reddy et al. 1995; Schepkin et al. 1998; Seo et al. 1990; Seshan et al. 1997; Tauskela et al. 1995), and tumors (Hancu et al. 2002; Winter and Bansal 2001; Winter et al. 2001). Some studies on cells or their fractions have also been reported, such as mitochondrial suspensions (Grieve et al. 1998), as well as human and dog red blood cells (RBCs) (Gullapalli et al. 1992; Knubovets et al. 1998; Shinar et al. 1993), human RBC ghosts (Knubovets et al. 1996) and human RBC membranes (Srinivasan et al. 1999).

Li^+ has been successfully used in the treatment of bipolar disorder, although its pharmacological mode and sites of action are still not completely clarified. ^{23}Na MQF NMR experiments have been performed in order to study Li^+/Na^+ binding competition in RBCs and RBC membranes (Gullapalli et al. 1992; Srinivasan et al. 1999). The binding state of Li^+ can be studied indirectly via the ^{23}Na multiple-quantum coherence as the ^7Li nucleus is only weakly quadrupolar and no ^7Li double quantum coherence can be detected (Gullapalli et al. 1991). The observed quenching of the ^{23}Na DQF NMR signal in both the intra- and extracellular compartments of human RBCs in the presence of Li^+ has been qualitatively interpreted by Li^+ competition with Na^+ for both intra- and extracellular binding sites in human RBCs (Gullapalli et al. 1992). Li^+ has also been shown to compete with Na^+ for binding sites in unsealed and cytoskeleton-depleted human RBC membranes (Srinivasan et al. 1999).

In this work we extended our previous membrane studies to quantitatively investigate the DQF and TQF ^{23}Na NMR behaviour of Na^+ in both intra- and extracellular compartments of a series of different types of cells, such as bovine chromaffin and human neuroblastoma SH-SY5Y cells, as well as rat neurons and astrocytes, and compared it with human RBCs in an effort to clarify the origin of the characteristics of the ^{23}Na MQF signal observed in tissues and organs. We also studied the Li^+/Na^+ competition for isotropic and anisotropic binding sites in those cell types through the effect of Li^+ loading on the DQF and TQF ^{23}Na cell signal. This detailed characterisation of the effect of Li^+/Na^+ competition in cells on Na^+ binding and dynamics are relevant to the interpretation of the in vivo pharmacokinetics and sites of Li^+ action.

Results

Li^+ cell uptake

Li^+ uptake by RBCs, astrocytes, chromaffin and SH-SY5Y cells incubated in the presence of Li^+ was followed by ^7Li NMR to establish the steady-state conditions of $[Li^+]_i$ for the ^{23}Na MQF experiments. Separation between the intra- and extracellular ^7Li NMR resonances was achieved using the paramagnetic SR $[Tm(HDOTP)]^{4-}$ at concentrations of 3 mmol l^{-1} (RBCs) or 5 mmol l^{-1} (astrocytes, chromaffin and SH-SY5Y cells). This SR remains in the extracellular space and shifts the extracellular ^7Li NMR resonance to higher frequencies relative to the intracellular ^7Li NMR resonance. The percentage of intracellular ^7Li resonance areas, normalised to the total area of intra- and extracellular signals, $(A_i/(A_i + A_e) \times 100)$, was calculated and plotted as a function of Li^+ loading time (Fig. S1). Li^+ influx rate constants, k_i, and the steady-state percentage of intracellular ^7Li resonance areas were calculated by fitting the data points to Eq. 3 and the results are summarised in Table 1.

Li^+ uptake by RBC suspensions (Ht = 47 %) at 25 °C, in the presence of $[Li^+]_{eT} = 40$ mmol l^{-1} Li^+, was found to be an extremely slow process, and the steady-state $A_i/(A_i + A_e)$ value was not reached during the time course of the influx experiment (6.5 h) (Fig. S1A). Due to the lack of enough data points to accurately define the influx curve, the steady-state values of $A_i/(A_i + A_e)$ and $[Li^+]_{if}$ and the k_i value could not be calculated accurately. However, we could calculate, using Eq. 2 with Ht = 47 % and $\alpha = 0.717$ (Gary-Bobo and Solomon 1968; Kirk et al. 1988; Savitz et al. 1964), that the RBCs accumulated $[Li^+]_{if} = 2.1$ mmol (L cells)$^{-1}$ after 6.5 h incubation. The $[Li^+]_{if}$ in RBCs reached after the ^{23}Na MQF experiments (see below) was calculated to be 3.4 mmol (L cells)$^{-1}$.

Li^+ uptake at 37 °C by agarose-embedded chromaffin and SH-SY5Y cells in the presence of 40 mmol l^{-1} Li^+, with time constant values, $k = 1/k_i$, of 1.54 ± 0.06 h and 1.15 ± 0.06 h, respectively, was found to be much faster than for RBC suspensions (Figs. S1B, S1C). The $[Li^+]_{if}$, calculated using Eq. 2, was 15.1 and 3.6 mmol (L cells)$^{-1}$ for chromaffin and SH-SY5Y cells, respectively, after 6.3 and 3.7 h of Li^+ incubation, very similar to the steady-state values [15.4 and 3.8 mmol (L cells)$^{-1}$, respectively]. A C_T of 41 % [chromaffin cells) and 56 % (SH-SY5Y cells) and α values of 0.45 [chromaffin cells (Fonseca et al. 2004)] and 0.874 [SH-SY5Y cells (Ahuja et al. 1978)] were used in these calculations. This latter α value refers to neuroblastoma cells in general and thus is only an estimate for the SH-SY5Y cells. The C_T value for these cells was calculated considering a similar total cell volume relative to chromaffin cells.

The kinetics of Li^+ influx, at 37 °C in BMG-immobilised astrocytes in the presence of 15 mmol l^{-1} Li^+, was found to be faster than observed for RBC suspensions and agarose-embedded chromaffin and SH-SY5Y cells, with a k value of 0.43 ± 0.01 h (Fig. S1D). However, it was not possible to calculate the value of $[Li^+]_{if}$ reached at steady state, since no α value for astrocytes could be found in the

Table 1 Li^+ influx rate constants (k_i), the steady-state $[Li^+]_{if}$ and the steady-state percentage of intracellular ^7Li resonance areas relative to the total area of intra- and extracellular ^7Li NMR resonances $A_i/(A_i + A_e)$ obtained for RBCs, chromaffin and SH-SY5Y cells, and rat astrocytes incubated in the presence of Li^+

Cell type	T (°C)	$[Li^+]_{eT}$ (mmol l^{-1})	k_i[a] (min^{-1})	$A_i/(A_i + A_e)$ (%)	$[Li^+]_{if}$ (mmol (L cells)$^{-1}$)
RBCs	25	40	[b]	[b]	2.1[c]
Chromaffin cells	37	40	0.0108 ± 0.0004[a]	10.9 ± 0.1	15.4
SH-SY5Y cells	37	40	0.0144 ± 0.0008[a]	9.6 ± 0.2	3.8
Astrocytes	37	15	0.0389 ± 0.0013[a]	6.6 ± 0.1	>16.0[d]

The steady-state $A_i/(A_i + A_e)$ values were extrapolated from the Li^+ influx curve and the steady-state $[Li^+]_{if}$ were calculated using Eq. 2

[a] Influx rate constants are apparent values (k_{iapp}) for the gel-embedded cells

[b] The values could not be obtained with accuracy

[c] $[Li^+]_{if}$ accumulated at 6.5 h

[d] Estimation of $[Li^+]_{if}$ taking into account that the α value must be <1 (see text)

literature. However, taking into account the C_T of 6 % used in these experiments, we can predict that $[Li^+]_{if}$ at steady state would be higher than 16 mmol (L cells)$^{-1}$, this latter value calculated using an hypothetical value of 1 for α in Eq. 2. As α must be lower than 1, due to the presence of membranes, organelles and cytosolic proteins, the $[Li^+]_{if}$ at steady state is certainly higher than 16 mmol (L cells)$^{-1}$.

^{23}Na DQF and TQF NMR of intra- and extracellular Na^+

In this work we used a TQF and DQF pulse sequence, with $\theta = 90°$ (TQF) or 54.7° ($DQF_{54.7}$), and the shift reagent $[Tm(HDOTP)]^{4-}$, to ensure the separate detection of the isotropic T_{31} and anisotropic T_{21} motions of Na^+ in the intra- and extracellular compartments. The creation time (τ) dependence of the ^{23}Na TQF and $DQF_{54.7}$ NMR signals obtained for the intra- and extracellular Na^+ ions in RBCs, chromaffin and SH-SY5Y cells, neurons and astrocytes incubated under control conditions, i.e., in the absence of Li^+, is shown in Figs. 1 and S2–S4. The observation of the intracellular ^{23}Na NMR resonance was achieved by separating the intra- and extracellular resonances using the SR $[Tm(HDOTP)]^{4-}$ at 5 mmol l^{-1} (except for RBCs, which was 3 mmol l^{-1}). A paramagnetic shift of the extracellular ^{23}Na NMR signal of +6.0, +5.5, +5.9, +6.8 and +4.4 ppm was observed in the ^{23}Na SQ spectra of RBCs, astrocytes, neurons, chromaffin and SH-SY5Y cells, respectively, before ^{23}Na MQF NMR spectra acquisition.

As expected, the TQF and $DQF_{54.7}$ ($\theta = 54.7°$) spectra consisted solely of positive T_{31} and negative T_{21} signals, respectively, thus allowing their separate detection. These components correspond, respectively, to the isotropic and anisotropic motions of Na^+ restricted by its binding sites. The intensities of the T_{31} and T_{21} components of the intra- and extracellular ^{23}Na MQF signals were modulated by the creation time. In all cases, extracellular Na^+ gave the dominant contribution to the $DQF_{54.7}$ spectra (Figs. 1b, d, S2B–S4B). In the TQF spectra, extracellular sodium dominated for RBCs (Fig. 1a) and to a lesser extent for chromaffin cells (Fig. S2A) and astrocytes (Fig. S4A). In SH-SY5Y cells, the intracellular and extracellular sodium had similar contributions (Fig. S3A), while in neurons, the intracellular sodium had the dominant contribution to the TQF spectra (Fig. 1c).

The modulation of the extracellular Na^+ T_{21} signals by the creation time was regular and very similar for the five types of cell systems (Figs. 1b, d, S2B–S4B), but the behaviour of the T_{31} signals was quite different for RBCs relative to chromaffin and SH-SY5Y cells (Figs. 1a, S2A, S3A). While the RBC suspensions gave an intense T_{31} signal with a regular modulation (Fig. 1a), the agarose-immobilised and perfused cells gave weak T_{31} signals with an irregular pattern of creation time dependence (Figs. S2A, S3A). This irregular pattern was not found in BMG-immobilised astrocytes (Fig. S4A) and neurons (Fig. 1c).

For intracellular Na^+, the ^{23}Na TQF spectra gave similar T_{31} signals in the five types of cell systems studied (Figs. 1a, c, S2A–S4A), with different intensities and creation time modulations (Figs. 2a, 3a, S5A–S7A), reflecting similar Na^+ binding to isotropic sites within the cells. However, differences in anisotropic intracellular Na^+ sites were detected since no T_{21} signals for intracellular Na^+ were observed for chromaffin cells (Figs. S2B, S5B), SH-SY5Y cells (Figs. S3B, S6B), astrocytes (Figs. 3b, S4B) and neurons (Figs. 1d, S7B), in contrast to RBCs where weak T_{21} signals in the $DQF_{54.7}$ spectra were detected (Figs. 1b, 3b).

Effect of Li^+ on the DQF and TQF ^{23}Na NMR signals of intra- and extracellular Na^+

The Li^+ loading of the RBCs, astrocytes, chromaffin and SH-SY5Y cells induced a small decrease as a function of

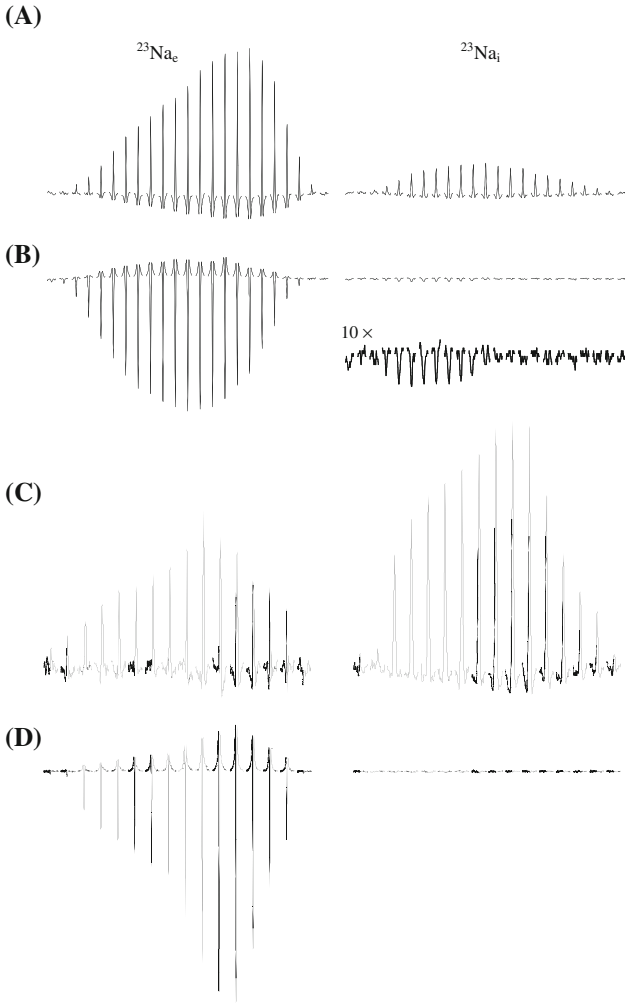

Fig. 1 ^{23}Na TQF (**a**, **c**) and $DQF_{54.7}$ (**b**, **d**) spectra (132.2 MHz, 37 °C) as a function of the creation time for RBCs suspended (**a**, **b**) and for rat neurons immobilised and perfused (**c**, **d**) with a medium containing no Li^+. T_{31} and T_{21} signals are shown for the extra- and intracellular ^{23}Na NMR resonances ($^{23}Na_e$ and $^{23}Na_i$, respectively). The creation time values used were as follows: 0.005, 0.05, 0.5, 1, 2, 3, 4, 5, 6, 7, 8, 9, 11, 13, 15, 17, 20, 25, 30, 40, 50, 70 and 100 ms (for **a**, **b**); 0.005, 0.05, 0.5, 0.8, 1, 1.2, 1.4, 1.6, 2.5, 3.75, 5, 10, 15, 20, 25 and 50 ms (for **c**, **d**)

time of the paramagnetic shift of the extracellular ^{23}Na SQ NMR signal induced by $[Tm(HDOTP)]^{4-}$ as a result of the competition of Li^+ and Na^+ ions for the same binding sites in the paramagnetic SR (Ramasamy et al. 1992). The Li^+ loading of the cells also affected the ^{23}Na SQ NMR signal intensities of the intra- and extracellular Na^+, reflecting a small change in the ionic distribution.

The effect of Li^+ on the ^{23}Na TQF and $DQF_{54.7}$ signals in the different cell systems was studied in order to evaluate the extent of Li^+/Na^+ competition in the intra- and extracellular environments. The measured TQF and $DQF_{54.7}$ signal intensities obtained under control and Li^+-loading conditions are shown in Figs. 2, 3, S5 and S6. These show that Li^+ loading has considerable effects on the ^{23}Na T_{31} and T_{21} signals from the extra- and intracellular environments of the different cellular systems studied, most of them being quenched in their maximum signal intensity, and for all the creation times used. However, in some cases an increase in signal intensity was observed, such as for the RBC intracellular T_{21} signal and astrocyte extracellular T_{31} signal, as well as for the extracellular T_{31} and T_{21} signals of the SH-SY5Y cells. Because Li^+ loading of the cells affects the SQ intensities and hence the intra- and extracellular Na^+ distribution, the quenching effect of Li^+ on the T_{31} and T_{21} signals can be quantitated by a comparison of the ^{23}Na TQF/SQ and $DQF_{54.7}$/SQ ratios, obtained from the maximum values of the TQF, $DFQ_{54.7}$ and SQ signal intensities for the intra- and extracellular Na^+ in the cells. Table 2 shows the TQF/SQ and $DQF_{54.7}$/SQ ratios obtained at τ_{max}, under control and Li^+ conditions, for RBCs, chromaffin and SH-SY5Y cells. These ratios were calculated taking into account the receiver gain, the number of acquisitions and the vertical scale used. In the absence of Li^+, the extracellular Na^+ ions gave the largest TQF/SQ and $DQF_{54.7}$/SQ ratios for RBCs in suspension, followed by the agarose-immobilised chromaffin and SH-SY5Y cells. For intracellular Na^+, while the TQF/SQ ratio was larger for SH-SY5Y cells, followed by chromaffin and RBCs, the $DQF_{54.7}$/SQ ratio was non-zero only in RBCs. The data in this table also show that, for extracellular Na^+, loading of RBCs with 40 mmol l^{-1} Li^+ quenched the isotropic T_{31} and anisotropic T_{21} signals by 42 and 21 %, respectively, while loading of chromaffin cells with the same Li^+ concentration induced a 21 % quenching of both T_{31} and T_{21} extracellular $^{23}Na^+$ signals. For SH-SY5Y cells there was an enhancement of T_{31} and T_{21} signals by 48 and 15 %, respectively. Furthermore, Table 2 indicates that, for intracellular Na^+, loading of RBCs with 40 mmol l^{-1} Li^+ decreased T_{31} by 12 % but enhanced T_{21} by 45 %, while loading of chromaffin and SH-SY5Y cells with the same Li^+ concentration quenched the T_{31} signal by 28 and 18 %, respectively.

The experimental points of the creation time (τ) dependence of the measured TQF and $DQF_{54.7}$ signal intensities (as given by their integrals), obtained for the intra- and extracellular compartments, under control and Li^+-loading conditions were fitted to Eqs. 4 and 5, respectively (Figs. 2, 3, S5 and S6). Tables 3 and 4 show the effect of Li^+ loading on the different parameters describing these signals, including the maximum intensity of the MQF (I_{max}) and the corresponding τ_{max}, the A and B constants, the T_{2f} and T_{2s} values and the residual quadrupolar coupling constant $\overline{\omega}_Q$, as well as the agreement factors R^2 defining the quality of the data fitting. As mentioned in the Methods section, in this analysis, in a first step, all the

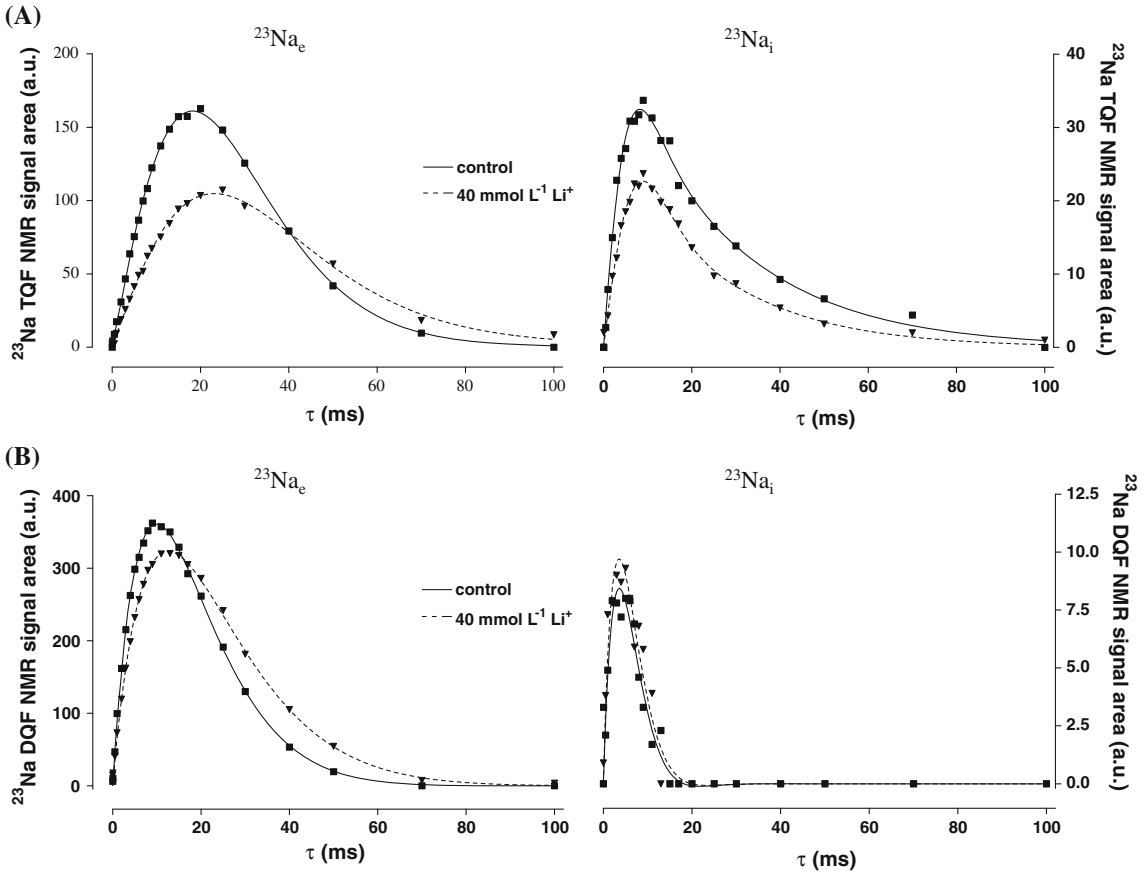

Fig. 2 ^{23}Na TQF (**a**) and $DQF_{54.7}$ (**b**) NMR signal areas versus creation time (τ) for human RBCs incubated in the absence (*square*, *plain line*) (control) and presence of 40 mmol l^{-1} Li^+ (*downward triangle*, *dashed line*) at 25 °C. Experiments were performed with the cells suspended in the experimental medium. Data points were fitted using Eqs. 4 and 5

parameters in Eqs. 4 and 5 were allowed to vary simultaneously. Then, in order to fine-tune the fitting procedure, $\overline{\omega}_Q$ was set to the best value(s) obtained in the previous optimisation step, and the data points were re-fitted by allowing the other parameters to vary. The R^2 values obtained indicate that the fits of the $DQF_{54.7}$ and the TQF data in general are excellent except for the TQF data for chromaffin cells and extracellular Na^+ in SH-SY5Y cells.

A general analysis of the data presented in these Tables shows that T_{2f} values for intracellular Na^+, obtained from T_{31} and T_{21} signals, are much smaller than for extracellular Na^+, in all cellular systems. In contrast, T_{2s} values for intracellular Na^+ are larger than for extracellular Na^+ in RBCs, astrocytes and neurons, but no relevant differences were observed in chromaffin and SH-SY5Y cells, which gave very large errors for this parameter. The $\overline{\omega}_Q$ values in RBCs were much larger for intracellular Na^+ than for extracellular Na^+, but for the other cell types there were no large differences in $\overline{\omega}_Q$ between intra- and extracellular Na^+, with values similar to extracellular Na^+ in RBCs.

Li^+ loading had no significant effect on $\overline{\omega}_Q$ in both compartments for all cell types. The effect of Li^+ on the other ^{23}Na T_{31} and T_{21} signal parameters was different for extra- and intracellular Na^+ ions. In the case of the extracellular compartment, the effects of Li^+ on T_{31} were (Table 3): (1) I_{max} decreased in RBCs, increased in SH-SY5Y cells and was not significantly affected in chromaffin cells and astrocytes; (2) τ_{max} increased in RBCs and SH-SY5Y cells and did not change in chromaffin cells and astrocytes; (3) T_{2f} and T_{2s} increased in RBCs and had no significant changes in the other three types of cells; (4) the A value decreased in RBCs, increased in SH-SY5Y cells and was not significantly affected in bovine chromaffin cells and astrocytes. The effect of Li^+ on the extracellular T_{21} signal was (Table 4): (1) I_{max} increased in SH-SY5Y cells and decreased in the other three types of cells; (2) τ_{max} increased in RBCs and did not change in the other cells; (3) T_{2f} increased in RBCs and slightly in astrocytes, did not change in SH-SY5Y cells and had a small decrease in chromaffin cells; (4) a decrease in B value was observed in RBCs and astrocytes, while an increase was detected in chromaffin and SH-SY5Y cells.

In the case of the intracellular compartment, the effect of Li^+ can be summarised as follows. For the T_{31} signal

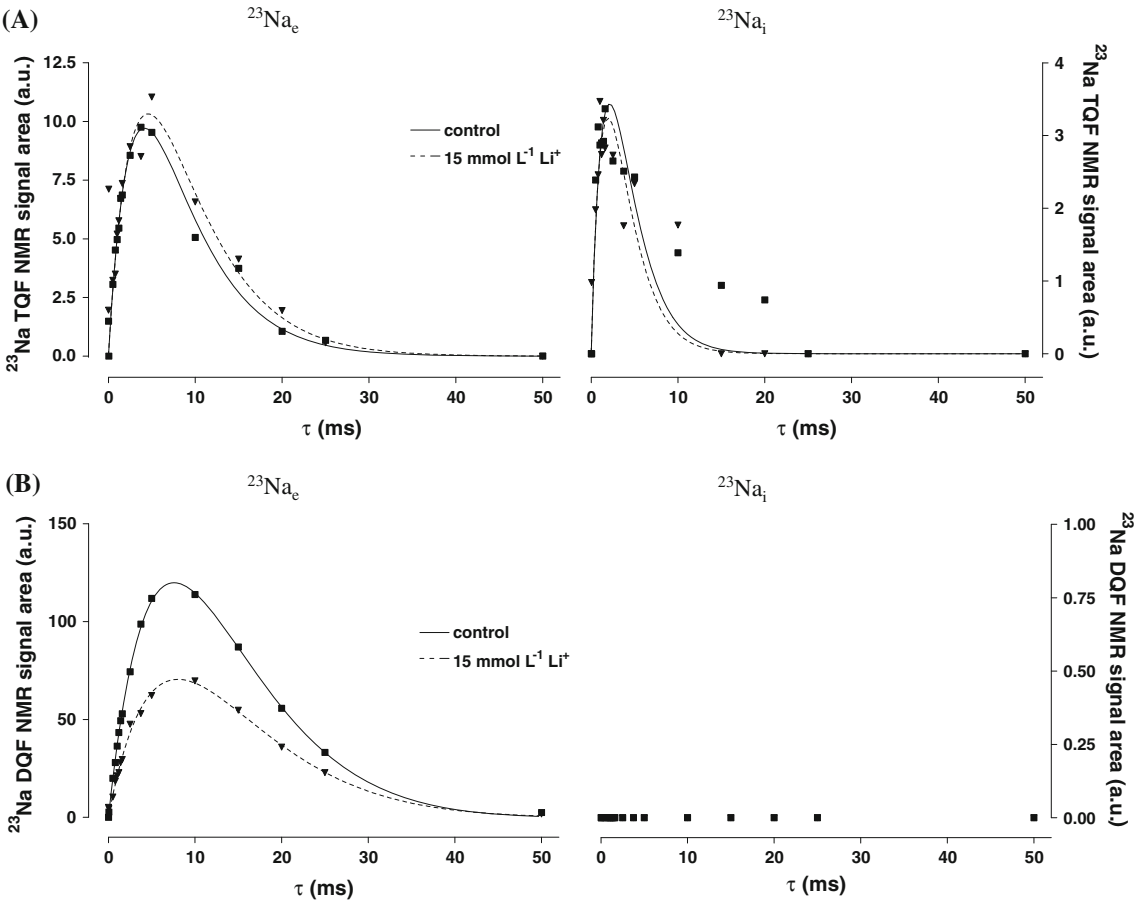

Fig. 3 ^{23}Na TQF (**a**) and $DQF_{54.7}$ (**b**) NMR signal areas versus creation time (τ) for astrocytes incubated in the absence (*square*, *plain line*) (control) and presence of 15 mmol l^{-1} Li^+ (*downward triangle*, *dashed line*) at 37 °C. Cells were immobilised in BMG threads and continuously perfused with the oxygenated and pH-adjusted experimental medium. Data points were fitted using Eqs. 4 and 5

Table 2 ^{23}Na TQF/SQ and $DQF_{54.7}$/SQ ratios (values × 10^{-3}), obtained from the maximum values of the ^{23}Na TQF and $DFQ_{54.7}$ signal areas, for the extra- and intracelullar Na^+ (Na_e^+ and Na_i^+, respectively) in three of the types of cells studied

Cell type	$[Li^+]_{eT}$	Na_e^+		Na_i^+	
	(mmol l^{-1})	TQF/SQ	$DQF_{54.7}$/SQ	TQF/SQ	$DQF_{54.7}$/SQ
RBCs	0	2.99	8.20	27.78	8.85
	40	1.72	6.49	24.39	12.82
Chromaffin	0	0.61	6.80	34.48	0[a]
	40	0.48	5.40	25.00	0[a]
SH-SY5Y	0	0.27	2.54	45.45	0[a]
	40	0.40	2.92	37.04	0[a]

The signal intensities were scaled to the same receiver gain, number of acquisitions and vertical scale

[a] $DQF_{54.7}$ signals have zero intensity

(Table 3): (1) a decrease in I_{max} values was observed for all systems except for astrocytes, which did not change; (2) τ_{max} was not affected for all systems; (3) T_{2f} increased in RBCs, while no significant changes were observed in the other cells; (4) T_{2s} had a small decrease in RBCs, increased for chromaffin cells and had no significant changes in SH-SY5Y cells and astrocytes; (5) the value of A decreased for all systems, except for astrocytes, where no relevant changes were observed. Regarding Li^+ effects on the intracellular T_{21} signal (Table 4), this study was restricted to RBCs, since no T_{21} signal could be detected for astrocytes, chromaffin and SH-SY5Y cells, as mentioned above. In RBCs, Li^+ slightly increased I_{max} and B values, and had no effect on τ_{max} and T_{2f}.

Discussion

In this work we used the $[Tm(HDOTP)]^{4-}$ SR to separate intra- and extracellular ^{7}Li and ^{23}Na resonances, allowing a preliminary kinetic study of Li^+ uptake by different types of cells by ^{7}Li SQ NMR. It also enabled us to monitor intra- and extracellular Na^+ binding and dynamics in those cellular systems, by ^{23}Na MQF NMR, and to understand

Table 3 ^{23}Na TQF NMR parameters, calculated from curve fitting using Eq. 4 for different types of cells, obtained before and after Li^+ incubation

Cell type	Compartment	$[Li^+]_{eT}$ (mmol l^{-1})	ω_Q (Hz)	A (a.u.)	T_{2f} (ms)	T_{2s} (ms)	I_{max} (a.u.)	τ_{max} (ms)	R^2
RBCs	Extracellular	0	9.3	798 ± 31	11.9 ± 0.1	15.5 ± 0.4	161.0	18.6	0.999
		40	8.1	353 ± 25	15.3 ± 0.2	24.0 ± 1.3	104.7	23.7	0.996
	Intracellular	0	31.8	44 ± 1	4.4 ± 0.2	26.0 ± 1.2	32.4	8.5	0.992
		40	31.2	32 ± 1	5.4 ± 0.2	22.4 ± 0.9	22.6	8.5	0.994
Chromaffin cells	Extracellular	0	6.4	57 ± 51	12.6 ± 3.2	25.1 ± 14.8	17.6	18.6	0.588
		40	10.4	29 ± 7	10.3 ± 2.1	39.0 ± 11.4	16.4	18.6	0.739
	Intracellular	0	6.4	10 ± 1	1.4 ± 0.3	21.6 ± 4.0	7.4	3.4	0.884
		40	6.4	6.5 ± 0.5	1.1 ± 0.2	30.9 ± 5.1	5.6	3.4	0.882
SH-SY5Y cells	Extracellular	0	6.4	6 ± 2	4.6 ± 2.9	67.0 ± 46.8	4.5	13.6	0.539
		40	6.4	14.4 ± 5.7	7.6 ± 2.8	36.4 ± 15.1	7.9	15.2	0.594
	Intracellular	0	6.4	15.1 ± 0.7	1.0 ± 0.1	20.3 ± 1.9	12.3	3.4	0.969
		40	6.4	13.0 ± 0.5	1.0 ± 0.1	20.8 ± 1.7	10.6	3.4	0.977
Astrocytes	Extracellular	0	9.5	27 ± 9	2.5 ± 0.4	6.8 ± 1.2	9.5	4.2	0.975
		15	9.5	26 ± 26	2.6 ± 1.5	7.8 ± 4.6	10.0	4.2	0.635
	Intracellular	0	6.4	3.6 ± 0.2	0.4 ± 0.1	10.5 ± 1.2	3.0	1.7	0.975
		15	6.4	3.8 ± 0.6	0.5 ± 0.2	7.7 ± 2.0	2.9	1.7	0.904
Neurons	Extracellular	0	9.5	14 ± 8	3.0 ± 0.8	7.3 ± 2.1	4.4	4.2	0.935
	Intracellular	0	9.5	10 ± 0.3	1.2 ± 0.1	13.7 ± 0.6	7.4	3.4	0.995

See text for fitting procedure details. I_{max}—maximum intensity of the ^{23}Na TQF spectra

Table 4 ^{23}Na $DQF_{54.7}$ NMR parameters, calculated from curve fitting using Eq. 5 for different types of cells, obtained before and after Li^+ incubation

Cell type	Compartment	$[Li^+]_{eT}$ (mmol l^{-1})	ω_Q (Hz)	B (a.u.)	T_{2f} (ms)	I_{max} (a.u.)	τ_{max} (ms)	R^2
RBCs	Extracellular	0	6.0	2,536 ± 21	10.5 ± 0.1	360.8	10.2	0.999
		40	4.5	2,418 ± 27	13.2 ± 0.1	322.7	11.9	0.998
	Intracellular	0	27.6	34 ± 3	4.2 ± 0.3	8.4	3.4	0.932
		40	25.1	44 ± 3	4.0 ± 0.2	9.7	3.4	0.954
Chromaffin cells	Extracellular	0	5.9	849 ± 28	14.3 ± 0.5	159.6	13.6	0.983
		40	4.8	1,033 ± 16	13.4 ± 0.2	149.8	13.6	0.996
	Intracellular	0	–	–	–	–	–	–
		40	–	–	–	–	–	–
SH-SY5Y cells	Extracellular	0	6.4	173 ± 10	14.6 ± 0.8	35.0	13.6	0.939
		40	6.4	235 ± 12	14.6 ± 0.8	47.4	13.6	0.944
	Intracellular	0	–	–	–	–	–	–
		40	–	–	–	–	–	–
Astrocytes	Extracellular	0	9.0	732 ± 6	8.1 ± 0.1	119.8	7.6	0.999
		15	8.1	456 ± 12	8.5 ± 0.2	70.4	7.6	0.989
	Intracellular	0	–	–	–	–	–	–
		15	–	–	–	–	–	–
Neurons	Extracellular	0	9.7	1,141 ± 5	8.51 ± 0.03	208.9	7.6	0.999
	Intracellular	0	–	–	–	–	–	–

See text for fitting procedure details. I_{max}—maximum intensity of the ^{23}Na $DQF_{54.7}$ spectra

how the presence of Li^+ may affect them, using the effects of Li^+/Na^+ ionic competition on the ^{23}Na DQF and TQF behaviour. In the absence of a SR, it is not possible to quantitatively distinguish between intra- and extracellular Na^+ by ^{23}Na MQF NMR (Dizon et al. 1996). The intra- and extracellular Li^+ resonances could also not be separated in the absence of the SR by ^7Li MQF NMR techniques because the multiple quantum coherences of this weakly quadrupolar nucleus are not detectable (Gullapalli et al. 1991). The conditions in which the SR was used do not significantly perturb the Li^+ and Na^+ cell transport kinetics and distribution (Fonseca et al. 2004; Layden et al. 2003; Nikolakopoulos et al. 1998). However, the SR on its own can lead to the appearance of DQF ^{23}Na signals even in the absence of slow motions and anisotropy because of cross-correlation between the paramagnetic and quadrupolar interactions (Ling and Jerschow 2007), which may affect the extracellular Na^+ MQF signals.

We started by studying the kinetics of Li^+ uptake by the cells and how it affects Na^+ distribution. As expected, the kinetics of Li^+ uptake depended on the specific cellular system under study (Fonseca et al. 2004; Layden et al. 2003; Nikolakopoulos et al. 1998). However, care should be taken when comparing the present k_i and steady-state $[Li^+]_i$ values with the ones reported in the literature. Differences in the experimental conditions, namely temperature, $[Li^+]_{eT}$, Ht (or C_T), cell manipulation (cells immobilised in agarose gel threads or in suspension) and the technique used for determining intracellular concentrations [NMR, which gives $[Li^+]_{if}$, or AA spectrophotometry, which gives the total intracellular Li^+ concentration ($[Li^+]_{iT}$)] could account for differences in the k_i and the steady-state $[Li^+]_i$ values (Fonseca et al. 2004; Gullapalli et al. 1991, 1992; Layden et al. 2003; Mota de Freitas et al. 1992).

Li^+ uptake by RBC suspensions (Ht = 47 %) at 25 °C, in the presence of 40 mmol l^{-1} Li^+, was an extremely slow process, of the order of several hours, in agreement with data published in the literature (Gullapalli et al. 1991, 1992). Under these conditions, RBCs accumulated 2.1 mmol (L cells)$^{-1}$ (3.2 % mole fraction of intracellular Li^+) after 6.5 h incubation. Gullapalli and co-workers reported, at 25 °C, Ht = 80 % and $[Li^+]_{eT}$ = 40 mmol l^{-1}, an accumulation of 11 % mole fraction of intracellular Li^+ (Gullapalli et al. 1992), which corresponds to $[Li^+]_{if} \sim 1.8$ mmol (L cells)$^{-1}$, a value smaller than the one found in the present work. This is not surprising since an increase in the Ht decreases the initial rate of Li^+ influx and the steady-state $[Li^+]_i$ (Mota de Freitas et al. 1992). At 25 °C, Ht = 85 % and $[Li^+]_{eT}$ = 50 mmol l^{-1}, a time constant value, k, of 16.5 h, corresponding to $k_i = 0.00101$ min^{-1}, was reported (Gullapalli et al. 1991), with an accumulation of 16.5 % mole fraction of intracellular Li^+, corresponding to $[Li^+]_{if} \sim 2.4$ mmol (L cells)$^{-1}$. This higher accumulation may be due to the increase in $[Li^+]_{eT}$ despite the higher Ht. Thus, the k_i value in our study at the lower Ht of 47 %, which could not be obtained (Table 1), should be even lower than the one reported in the literature, as k_i decreases with decreasing Ht (Mota de Freitas et al. 1992).

It should be noticed that the k_i values determined for the immobilised cells are in fact apparent k_i (k_{iapp}) because of the contribution of the diffusion process of Li^+ across the gel before reaching the cells (Fonseca et al. 2004; Nikolakopoulos et al. 1996). The k_{iapp} value obtained in this study for chromaffin cells immobilised in agarose gel threads ($k_{iapp} = 0.0108 \pm 0.0004$ min^{-1} or $k = 1.54 \pm 0.06$ h, at $[Li^+]_{eT}$ = 40 mmol l^{-1}) is unexpectedly similar to the value reported for perfusion with a lower $[Li^+]_{eT}$ = 15 mmol l^{-1} ($k_{iapp} = 0.012 \pm 0.003$ min^{-1}, $k = 1.39 \pm 0.35$ h) (Fonseca et al. 2004). However, the steady-state $[Li^+]_{if}$, determined by ^7Li NMR, decreased with the concentration of Li^+ in the extracellular medium: $[Li^+]_{if}$ = 15.4 mmol l^{-1} (cells)$^{-1}$ for $[Li^+]_{eT}$ = 40 mmol l^{-1} Li^+ (present work) versus $[Li^+]_{if}$ = 9.4 mmol l^{-1} (cells)$^{-1}$ for $[Li^+]_{eT}$ = 15 mmol l^{-1} Li^+ (Fonseca et al. 2004). This indicates that diffusion across the gel limits the kinetic constant for Li^+ uptake by the cells, but not the amount of Li^+ available for intracellular accumulation.

Concerning SH-SY5Y cells, the values obtained in the present work using ^7Li NMR and agarose immobilised cells ($k_{iapp} = 0.0144 \pm 0.0008$ min^{-1} or $k = 1.16 \pm 0.06$ h, and steady-state $[Li^+]_{if}$ = 3.8 mmol (L cells)$^{-1}$) were lower than the ones obtained by AA spectrophotometry in SH-SY5Y cell suspensions (C_T = 1–5 %) incubated in the presence of 50 mmol l^{-1} Li^+ ($k_i \sim 0.040$ min^{-1} or $k = 0.42$ h, and steady-state $[Li^+]_{iT}$ = 12.6 mmol (L cells)$^{-1}$) (Layden et al. 2003). The lower intracellular Li^+ concentration obtained in the present work was predictable because of the lower extracellular Li^+ concentration used (40 mmol l^{-1}) and the fact that only free intracellular Li^+ ions are visible by NMR. The lower k_i value was also expected since Li^+ influx kinetics are faster in cell suspensions than in cells immobilised in agarose gel threads because of the diffusion of Li^+ across the gel (Fonseca et al. 2004). Studies of Li^+ kinetics in agarose-embedded SH-SY5Y cells have also been reported, but using a smaller extracellular Li^+ concentration (15 mmol l^{-1}). Under those conditions, the kinetics of Li^+ influx were faster ($k_{iapp} = 0.055 \pm 0.006$ min^{-1}, determined by ^7Li NMR) but the cells accumulated less Li^+ after 5 h of Li^+ influx ($[Li^+]_{iT}$ = 2.9 mmol (L cells)$^{-1}$, determined by AA spectrophotometry), probably because of the lower extracellular Li^+ concentration (Nikolakopoulos et al. 1998). The difference in k_{iapp} may be due to differences in the compactation of gel threads in the NMR tube. We have found that a higher compactation degree of the gel threads in the NMR tube is

associated with lower influx rate constants (data not shown). In our experiments, agarose gel threads in the NMR tube were highly compacted in the detection region of the NMR probe in order to improve the signal-to-noise ratio, which may have slowed Li^+ diffusion across the gel, leading to lower k_{iapp} values.

A faster kinetics of Li^+ influx was found in BMG-immobilised astrocytes, at 37 °C, in the presence of 15 mmol l^{-1} Li^+ when compared to RBC suspensions and agarose-embedded chromaffin and SH-SY5Y cells ($k = 0.43 \pm 0.01$ h, which corresponds to $k_{iapp} = 0.0389 \pm 0.0013$ min^{-1}). This may in part result from the lower rigidity and higher ion permeability of the BMG threads relative to the agarose threads, allowing a faster diffusion of Li^+ to the astrocytes embedded in them. Besides the faster kinetics, the BMG-immobilised astrocytes also accumulated the highest Li^+ concentration when compared to the other cellular systems.

The ^{23}Na TQF and $DQF_{54.7}$ spectra, along with the use of the SR $[Tm(HDOTP)]^{4-}$, allowed the separate detection of the isotropic (T_{31}) and anisotropic (T_{21}) motions of the extra- and intracellular Na^+ restricted by its binding sites. For intracellular Na^+, the TQF spectra gave similar T_{31} signals for the five types of cells, reflecting similar isotropic motions, but the $DQF_{54.7}$ spectra gave T_{21} signals only for RBCs, reflecting differences in anisotropic intracellular Na^+ sites. This correlates very well with the much larger $\overline{\omega}_Q$ values determined for intracellular Na^+ in RBCs than in other cell types (see later). Anisotropic motions of intracellular Na^+, resulting in a residual quadrupolar interaction, have been associated with Na^+ binding to the cytoskeleton proteins, in particular the spectrin fibers, the major component of the RBCs membrane skeleton (Knubovets et al. 1996; Shinar et al. 1993). Such anisotropic binding sites were also observed in other biological systems (Navon et al. 2001), such as connective tissues (e.g. skin, cartilages) (Borthakur et al. 2002; Duvvuri et al. 1998; Eliav and Navon 1994; Eliav et al. 1992; Insko et al. 1999; Reddy et al. 1997; Shinar et al. 1995), for which the effect resulted from Na^+ interaction with the collagen fibres (Eliav and Navon 1994; Eliav et al. 1992; Shinar et al. 1995), and also in other tissues, such as perfused rat hearts (Schepkin et al. 1998; Tauskela et al. 1995), rat brain (Lyon et al. 1991) and in vivo human skeletal muscle, brain (Reddy et al. 1995) and breast (Duvvuri et al. 1999). The absence of anisotropic Na^+ motions within neurons, astrocytes, chromaffin and SH-SY5Y cells probably results from the lack of binding of Na^+ to fibrous structures in their cytoplasm or to the different organisation or protein composition of the cytoskeleton. For instance, distinct isoforms of spectrin (namely fodrin, a spectrin-like nonerythroid protein) were found to be present in chromaffin cells and brain in general (Fujimoto et al. 1991; Hays et al. 1994; Langley et al. 1986).

The patterns observed for the extracellular T_{31} and T_{21} signals in the RBC suspensions result from the binding of extracellular Na^+ by the outer cell membrane surface, but in the immobilised cells the heterogeneity of the extracellular medium caused by the presence of the agarose gel contributes to the immobilisation of the Na^+ ions, which are present in distinct environments with different mobilities. This heterogeneity affects the isotropic Na^+ sites, leading to the irregular pattern of the T_{31} signals observed, but does not affect the anisotropic sites reflected by the T_{21} signals, which could come predominantly from membrane-binding sites. This irregular pattern was not found in BMG-immobilised astrocytes and neurons, probably because of the lower rigidity and higher ion permeability of the BMG threads relative to the agarose threads.

The present studies on RBC suspensions at Ht = 47 % can be compared with previous studies with Ht = 88 and 58 % (Knubovets et al. 1998). While the transverse relaxation parameters, T_{2f} and T_{2s}, of the intracellular $^{23}Na^+$ SQ resonance are basically not affected by the presence of the SR or a change of Ht, those of the extracellular Na^+ are dependent on these two factors (Knubovets et al. 1998). These parameters determine the values of τ_{max}, and also the efficiency of the MQF signals, as given by the ratio of MQF_{max}/SQ intensities. In fact, the MQF_{max}/SQ ratio depends on the relaxation rate ratio R_{2f}/R_{2s}, with $R_{2f} = 1/T_{2f}$ and $R_{2s} = 1/T_{2s}$ (Tauskela and Shoubridge 1993). For Ht = 47 %, we obtained values of τ_{max} of 3.4 ms ($DQF_{54.7}$) and 8.5 ms (TQF) for intracellular Na^+ (Tables 3, 4), in good agreement with the literature values at Ht = 88 and 58 % (Knubovets et al. 1998). For extracellular Na^+, at Ht = 47 % and 3.0 mmol l^{-1} $[Tm(HDOTP)]^{4-}$, we obtained τ_{max} of 10.2 ms ($DQF_{54.7}$) and 18.6 ms (TQF), compared with τ_{max} of 7.0 and 2.4 ms ($DQF_{54.7}$), and about 5.0 and 5.0 ms (TQF) at Ht = 58 and 88 %, respectively, with 2.3 mmol l^{-1} $[Tm(HDOTP)]^{4-}$ (Knubovets et al. 1998). Thus, an increase of Ht decreases the value of τ_{max} for extracellular Na^+, as both T_{2f} and T_{2s} decrease as a result of an increase in the percentage of extracellular Na^+ bound at the outer cell membrane (Knubovets et al. 1998). The fraction of bound Na^+ is one of the factors determining the $T_{2s}/T_{2f} = R_{2f}/R_{2s}$ ratio, which, as discussed above, is a factor determining the efficiency of the multiple-quantum filtering and thus the MQF_{max}/SQ intensities. The well-known reduction of the extracellular MQF signal intensity due to the presence of the SR (Jelicks and Gupta 1989a) results from its paramagnetic effect on the relaxation of the extracellular ^{23}Na, which tends to equalise the T_{2f} and T_{2s} values.

The extracellular Na^+ gave the largest TQF/SQ and $DQF_{54.7}/SQ$ ratios for RBCs in suspension, followed by the agarose-immobilised chromaffin and SH-SY5Y cells.

As discussed above, chromaffin and SH-SY5Y cells gave strong T_{21} signals but weak and irregular T_{31} signals, reflecting the strongly restricted anisotropic motions of the extracellular Na^+ ions by the gel threads, leaving little contribution to isotropic motions. For intracellular Na^+, while the TQF/SQ ratio was largest for SH-SY5Y cells, followed by chromaffin and RBCs, the $DQF_{54.7}$/SQ ratio was non-zero only in RBCs. This reflects the importance of the intracellular Na^+ anisotropic motions in RBCs, restricted by the presence of the specific cytoskeleton proteins (Knubovets et al. 1996; Tauskela and Shoubridge 1993), which may be absent or present in different isoforms in the cytoplasm of the other cells, only with isotropic Na^+ motions.

We found that Li^+ loading had considerable effects on the ^{23}Na TQF and $DQF_{54.7}$ signals from the extra- and intracellular compartments of the different cellular systems studied. A quenching of the ^{23}Na DQF NMR signal in both intra- and extracellular compartments of human RBCs in the presence of Li^+ has been observed before (Gullapalli et al. 1992), and this was presented as evidence for competition of Li^+ with Na^+ for both intra- and extracellular binding sites in human RBCs. However, in that study the pulse sequence used to generate the DQF had a value of $\theta = 90°$ (DQF_{90}), which generates a superposition of signals from the second (T_{21}) and third (T_{31}) rank tensors with relative contributions that vary with the creation time τ, leading to large variations of line shape with the τ value, as also observed by us (data not shown) (Knubovets et al. 1996, 1998; Shinar et al. 1993; Tauskela and Shoubridge 1993). Thus, the failure to account for the T_{21} contributions strongly affected the signal integration (Tauskela and Shoubridge 1993), especially at low τ values, and thus the whole analysis of the data. In this work, we used the TQF ($\theta = 90°$) and $DQF_{54.7}$ ($\theta = 54.7°$) to ensure the separate detection of the T_{31} and T_{21} contributions.

The values of $\overline{\omega}_Q$ for extracellular Na^+, obtained from the T_{31} and T_{21} signals, agreed well for each cell type, and also in the five types of cellular systems studied (7.8 ± 1.9 Hz). The $\overline{\omega}_Q$ values for intracellular Na^+ were much larger for RBCs (29 ± 3 Hz) than for the other types of cells studied (8.0 ± 1.6 Hz), indicating that the partially averaged anisotropies of the Na^+ binding sites in the intracellular medium of RBCs are much higher than for other cells. They were also much higher than for extracellular Na^+ in all cases. The $\overline{\omega}_Q = 29 \pm 3$ Hz value obtained in this work for intracellular Na^+ in RBCs agrees quite well with the value of 25 Hz reported in the literature (Tauskela and Shoubridge 1993).

The quantitative assessment of the quenching effect of Li^+ on the ^{23}Na NMR T_{31} and T_{21} signals could in principle be done by comparison of I_{max}, TQF/SQ and $DQF_{54.7}$/SQ, or A and B amplitudes. The MQF signal efficiencies, given by the MQF_{max}/SQ values (Table 2), depend on the R_{2f}/R_{2s} ratio, which is believed to also reflect the fraction of bound Na^+ (Tauskela and Shoubridge 1993). In fact, the use of the DQF_{90} pluse sequence in early studies, giving both T_{21} and T_{31} signals, led to reports that the efficiency of the generation of a DQF signal varies with the physiological state, thus preventing the quantitation of intracellular Na^+ concentration ($[Na^+]_i$) in biological systems by this methodology. For instance, changes in the DQF intracellular $^{23}Na^+$ intensity were not found to be proportional to changes of $[Na^+]_i$ in human RBCs (Gullapalli et al. 1992; Jelicks and Gupta 1989b) and in perfused rat hearts (Hutchison et al. 1993). Signal quenching in these systems was attributed to a reduction in macromolecular Na^+ binding sites, due to an increased ratio of $Na^+_{(free)}/Na^+_{(bound)}$ ions (Jelicks and Gupta 1989b), competition with Li^+ for a limited number of binding sites (Gullapalli et al. 1992) or a qualitative change in macromolecular Na^+ binding (Hutchison et al. 1993). However, a later study has shown that, by isolating the contribution from T_{31} exclusively, the DQF/SQ ratio for intracellular Na^+ in human RBCs was constant over a fourfold change of $[Na^+]_i$ produced by addition of nystatin, leading to a proposal that DQF/SQ is invariable with the physiological state (Tauskela and Shoubridge 1993). We found in our study that the effect of Li^+ is not the same on I_{max}, MQF_{max}/SQ, R_{2f}/R_{2s} and A (or B) for each experimental condition, reflecting the complexity of Eqs. 4 and 5. For example, in the case of extracellular Na^+ in RBCs, Li^+ addition causes an increase in the R_{2f}/R_{2s} ratio, but all the T_{31} intensity parameters (I_{max}, TQF_{max}/SQ and A), as well as the T_{21} parameters (I_{max}, DQF_{max}/SQ and B) decrease, indicating a quenching of both MQF signals. Thus, following a previous ^{23}Na MQF NMR study of Li^+/Na^+ competition for the interaction with RBC membranes (Srinivasan et al. 1999), we used the changes in the intensities of A and B as a measure of the quenching effect of Li^+ on the $^{23}Na^+$ T_{31} and T_{21} signals.

Using this simple approach, we found that Li^+ binding quenched the extracellular Na^+ MQF signals in some cases, like T_{31} (56 %) and T_{21} (5 %) of RBCs, T_{31} (33 %) of chromaffin cells (although this may not be relevant since the errors are quite large) and T_{21} (38 %) of astrocytes, but it also increased their intensities in other cases, namely T_{21} (22 %) of chromaffin cells, and both T_{31} (160 %) and T_{21} (36 %) of SH-SY5Y cells. The effects on the RBC suspensions simply reflect the competition of Li^+ with Na^+ ions for both isotropic and anisotropic binding sites at the extracellular surface of the RBC membrane. However, the more complex effects observed for extracellular Na^+ in the agarose-embedded cell systems reflect, besides that

competition, the effect of Li^+ on the Na^+ isotropic and anisotropic movements at the gel surface.

The effects of Li^+ on intracellular Na^+ MQF signals are physiologically more interesting. In RBCs, Li^+ quenches intracellular Na^+ T_{31} signals by 27 % but enhances T_{21} by 29 %, indicating that intracellular Li^+/Na^+ competition in RBCs decreases the Na^+ isotropic movements but enhances its anisotropic motions, which are promoted by the cytoskeleton proteins. This enhancing effect of Li^+ on the anisotropy of Na^+ movements related to the cytoskeleton of RBCs is in agreement with previous observations in RBC membranes (Srinivasan et al. 1999). For the other cell systems, which lack the T_{21} signal, possibly because of a different organisation and protein composition of the cytoskeleton, we observed a quenching of T_{31} for chromaffin (28 %) and SH-SY5Y (14 %) cells, reflecting the effects of Li^+ on the intracellular Na^+ isotropic movements. However, no effect was observed for astrocytes, possibly because of the lower Li^+ concentration used in these experiments.

Conclusions

The study of the effect of Li^+ on the ^{23}Na TQF and $DQF_{54.7}$ NMR signals in different cellular systems allowed a detailed evaluation of the Li^+/Na^+ competition in the intra- and extracellular environments. Li^+ was found, in most cases, to interfere with the intra- and extracellular anisotropic and isotropic Na^+ motions. In particular, Li^+ loading decreased intracellular Na^+ isotropic movements in all types of cells (except in astrocytes incubated with a lower Li^+ concentration) and increased the anisotropic Na^+ movements in RBCs. Differences in cytoskeleton composition or organisation may explain the absence of intracellular $^{23}Na^+$ T_{21} signals in chromaffin cells, SH-SY5Y cells and astrocytes compared to RBCs. These effects of Li^+ on the intracellular ^{23}Na MQF signals are of physiological interest, in particular taking into account that efficient imaging schemes have allowed the acquisition of TQF ^{23}Na magnetic resonance images in the in vivo brain within clinically acceptable data acquisition times, which has allowed the study of early increases of intracellular Na^+ during brain ischemia in live non-human primates (LaVerde et al. 2007). Li^+ effects on the extracellular ^{23}Na MQF signals are more complex since they can reflect Li^+/Na^+ competition for both isotropic and anisotropic binding sites at the extracellular surface of cell membranes, but also at the gel surface (in the case of gel-immobilised cells). In fact, the introduction of another Na^+ compartment by the presence of a gel matrix to which Na^+ can bind will contribute to those ^{23}Na MQF signals. The presence of the SR can partially quench the extracellular DQF ^{23}Na signals (Jelicks and Gupta 1993), but also contribute to the appearance of DQF ^{23}Na signals in the extracellular compartment(s) because of cross-correlation between the paramagnetic and quadrupolar interactions (Ling and Jerschow 2007). In summary, ^{23}Na MQF NMR spectroscopy, along with the SR $[Tm(HDOTP)]^{4-}$, was found to be a powerful tool for the detailed study of extra- and intracellular molecular sites of Na^+ and Li^+ binding, enabling the distinction between isotropic and anisotropic Na^+ binding sites and the study of the extent of Li^+ competition for those sites.

Materials and methods

Materials

Collagenase (type *B*) and Percoll were purchased, respectively, from Boehringer Mannheim (Mannheim, Germany) and Pharmacia Biotech AB (Uppsala, Sweden). The shift reagent (SR) $Na_3H_2Tm(DOTP).3NaCl$ was obtained from Macrocyclics (Richardson, Texas, USA). Dulbecco's modified Eagle's medium (DMEM)/Ham's nutrient mixture F-12 (DMEM/F-12, 1:1 mixture) was purchased from GibcoBRL Life Technologies (Gaithersburg, MD, USA). DMEM, Eagle's basal medium (BME) and fetal bovine serum (FBS) were purchased from GIBCO (Glasgow, UK). Culture dishes and flasks were obtained from Nunc (Roskilde, Denmark). Matrigel solution was from Serva (Heidelberg, Germany). All other reagents were obtained from Sigma (St. Louis, MO, USA) or Merck (Darmstadt, Germany).

Preparation of human red blood cell suspensions

Human venous blood was drawn into glucose-citrate anticoagulant containing tubes (1 ml of glucose-citrate anticoagulant for 6 ml of blood) and used immediately. The pellet of RBCs was separated from plasma by centrifugation at $3{,}100\times g$ for 10 min, 4 °C (Sigma 3K10), and washed three times in ice-cold saline isotonic solution (0.9 % NaCl). The RBC pellet was then re-suspended in an equal volume of a cold buffer containing, in mmol l^{-1}, NaCl 140, KCl 5, glucose 10 and *N*-2-hydroxyethylpiperazine-*N*′-2-ethanesulfonic acid (HEPES) 10, pH 7.35. The hematocrit of each sample was found to be 45–47 %. The cell suspension (2 ml) was then placed in a 10-mm outer diameter (o.d.) NMR tube for the NMR experiments.

Isolation of bovine chromaffin cells

Chromaffin cells were isolated from bovine adrenal medulla by collagenase *B* digestion and purified on a

continuous Percoll density gradient, as described before (Brocklehurst et al. 1990). The cells were cultured up to a density of 1×10^6 cells ml^{-1} in a 1:1 mixture DMEM/F-12 (1.56 %) medium buffered with 15 mmol l^{-1} HEPES and 26 mmol l^{-1} $NaHCO_3$, supplemented with 5 % (v/v) of heat-inactivated FBS, 100 units ml^{-1} of penicillin, 100 µg ml^{-1} of streptomycin and 0.25 µg ml^{-1} of amphotericin *B*, at 37 °C, in a humidified CO_2 (5 %) and air (95 %) atmosphere. After 3 days in culture, chromaffin cells (90×10^6 cells, approximately) were collected and centrifuged at $115 \times g$ for 8 min at room temperature (Sigma 3K10). The cells were then immobilised in agarose gel threads (final agarose concentration of 1 %) with 0.5 mm external diameter, as described previously (Fonseca et al. 2004; Montezinho et al. 2002) and placed in a 10-mm o.d. NMR tube and perfused, at 1 ml min^{-1}, with oxygenated culture medium (37 °C) for the NMR experiments.

Preparation of human neuroblastoma SH-SY5Y cells

The human neuroblastoma SH-SY5Y cell line was provided by Dr. E. Stubbs, Jr. (Department of Neurobiology, Loyola University Medical Center). The cells were grown at 37 °C in a humidified CO_2 (5 %) and air (95 %) atmosphere in DMEM buffered with 18 mmol l^{-1} $NaHCO_3$, pH 7.35, and supplemented with 10 % (v/v) FBS, 100 units ml^{-1} of penicillin and 100 µg ml^{-1} of streptomycin. When a confluence of 90 % was achieved, the cells ($100–200 \times 10^6$ cells) were harvested with Puck's D_1 solution (in mmol l^{-1}: glucose 5, sucrose 58, NaCl 137, Na_2HPO_4 0.2, KH_2PO_4 0.2, KCl 5, pH 7.35) and immobilised in agarose gel threads (final agarose concentration of 0.75 %) with 0.5-mm external diameter, as reported in the literature (Fonseca et al. 2004; Montezinho et al. 2002). The gel threads containing the cells were collected directly into a 10-mm o.d. NMR tube and perfused, at 1 ml min^{-1}, with oxygenated culture medium (37 °C) for the NMR experiments.

Isolation of rat neuronal cells

Single cell suspensions were prepared from 16-day-old embryos from Wistar rats as described previously (Richter-Landsberg 1988). The cerebral hemispheres from 14 to 16 embryos were freed of meninges and mechanically disrupted. Cells were sedimented by centrifugation, re-suspended in 1 ml BME containing 10 % FBS and immediately mixed with 1 ml of basement membrane gel (BMG) extract (matrigel solution). Gel threads (0.3-mm diameter) were made, as described earlier (Alves et al. 1996), into culture dishes containing BME medium supplemented with 10 % FBS and penicillin/streptomycin (100 units ml^{-1}) and incubated at 37 °C, in a humidified atmosphere of 10 % CO_2 in air, for 2–3 h, after which, the culture medium was exchanged to BME containing 0.5 % FBS (Brand et al. 1997). The cells were then incubated for 5 days and used for NMR experiments. Cell growth inside the threads was followed using an inverted microscope. For NMR experiments, neurons immobilised in BMG threads were transferred into a 10-mm o.d. NMR tube fitted with a perfusion insert (Alves et al. 1996; Flogel et al. 1994). Typical amounts of biomass corresponded to 70 µg of DNA per experiment for neurons. Cells were perfused at 1–1.5 ml min^{-1} with BME containing 0.5 % FBS and 1 g l^{-1} of glucose at 37 °C and continuously gassed with 95 %O_2/5 %CO_2.

Isolation of rat astrocytes

Primary cultures of astrocytes were prepared from 1- to 2-day-old Wistar rats as described before (Richter-Landsberg and Besser 1994). In brief, cerebral hemispheres were freed of the meninges, mechanically disrupted and plated on culture flasks (2 brains/175 cm^2). Cells were kept for 6–8 days in DMEM supplemented with 10 % FBS and penicillin/streptomycin (100 units ml^{-1}) at 37 °C in an incubator with a humidified atmosphere of 7 % CO_2 in air. After 8 days of preculturing, the phase dark cells were separated by vigorous shaking and removed as previously described (McCarthy and de Vellis 1980). The remaining astrocytes were detached by mild trypsinisation and subcultured in T-flasks for another 25 days. The growth medium was changed twice a week. After this period of time, approximately 10^7 cells were harvested by trypsinisation and pelleted by centrifugation. The cells were then re-suspended in 1 ml of DMEM and immobilised in BMG threads that were placed in culture dishes filled with culture medium and kept for 5 days in the incubator (Alves et al. 1996; Daly et al. 1988). Cell growth inside the threads was followed using an inverted microscope. For NMR experiments, astrocytes immobilised in BMG threads were transferred into a 10-mm o.d. NMR tube fitted with a perfusion insert (Alves et al. 1996; Flogel et al. 1994). Typical amounts of biomass corresponded to 100 µg of DNA per experiment for astrocytes. Cells were perfused at 1–1.5 ml min^{-1} with DMEM containing 0.5 % FBS and 1 g l^{-1} of glucose at 37 °C and continuously gassed with 95 %O_2/5 %CO_2.

NMR experiments

^{23}Na single quantum (SQ) and MQF NMR spectra were acquired in the absence and in the presence of 3 mmol l^{-1} (RBCs) or 5 mmol l^{-1} (astrocytes, chromaffin and SH-SY5Y cells) of the paramagnetic SR thulium(III)-1,4,7,10-

tetrazacyclododecane-*N*,*N*′,*N*″,*N*‴-tetramethylenephosphonate ([Tm(HDOTP)]$^{4-}$), pH 7.35, in order to separate the intra- and extracellular $^{23}Na^{+}$ resonances. ^{23}Na SQ and MQF NMR spectra were acquired before Li^{+} addition to the experimental medium (control) in all types of cells studied. In the case of RBCs, chromaffin cells, SH-SY5Y cells and astrocytes, these spectra were also obtained after Li^{+} influx into the cells, when the steady-state intracellular Li^{+} concentration, $[Li^{+}]_i$, was reached (except for RBC experiments where a steady state could not be reached).

Li^{+} uptake by RBCs, astrocytes, chromaffin and SH-SY5Y cells was followed by ^{7}Li NMR spectroscopy along with the SR [Tm(HDOTP)]$^{-4}$ (see concentrations above). LiCl was added to the suspension or perfusate medium to reach a final concentration of 15 or 40 mmol l^{-1}. For astrocytes, chromaffin and SH-SY5Y cells, Li^{+} added to the perfusate was first allowed to equilibrate with the extracellular medium, usually for 7–8 min, and the influx experiment was considered to start (time zero) when the amount of extracellular $^{7}Li^{+}$ in the NMR tube became constant, as monitored by consecutive single acquisitions of ^{7}Li NMR spectra. Li^{+} was then allowed to diffuse into the cells for 6.5 h (RBCs), 6.3 h (chromaffin cells), 3.7 h (SH-SY5Y cells) and 2.5 h (astrocytes).

NMR spectral conditions

NMR experiments were recorded at 37 °C (except for RBCs, where the assays were performed at 25 °C) using 10-mm o.d. NMR tubes and the samples were not spun.

NMR experiments on RBC suspensions, perfused immobilised bovine chromaffin cells and human neuroblastoma SH-SY5Y cells were performed on a Varian Unity 500 NMR spectrometer equipped with a multinuclear 10-mm broadband probe and a controlled temperature unit. NMR spectra of primary astrocytes and neurons immobilised in BMG threads were acquired on a Bruker DRX500 NMR spectrometer using a 10-mm broadband probe. The two spectrometers were operating at a resonance frequency of 132.2 MHz for ^{23}Na and 194.3 MHz for ^{7}Li.

Typically, ^{7}Li NMR spectra were acquired on the Bruker spectrometer with 16 transients, a standard 90° pulse, an interpulse delay time of 9.6 s and an acquisition time of 1.4 s. In the two cases, the signal-to-noise ratio was enhanced by exponential multiplication with a line broadening of 10 Hz. On the Varian spectrometer, each ^{7}Li NMR spectrum was obtained from 64 transients (total accumulation time of 11 min for each spectrum) with a standard 90° pulse (pulse width of 15 μs), a spectral width of 5,600 Hz, an interpulse delay time of 10 s and an acquisition time of 0.360 s.

The ^{23}Na SQ NMR spectra were acquired with a standard 90° pulse calibrated for each sample (pulse width between 18 and 19 μs), a spectral width of 7,000 Hz, an acquisition time of 475 ms and an interpulse delay time of 1 s. The signal-to-noise ratio was enhanced by exponential multiplication with a line broadening of 10 Hz. For each sample, the receiver gain of the instrument was set to an appropriate value in order to avoid signal overflow.

The DQF and TQF T_2 spectra were acquired with the pulse sequence

$$90^\circ - \tau/2 - 180^\circ - \tau/2 - \theta^\circ - \delta - \theta^\circ - t\,(\text{acquisition}) \quad (1)$$

using a 128-step phase cycling routine with $\theta = 54.7°$ or 90° for $DQF_{54.7}$ or DQF, respectively, and a 384-step routine with $\theta = 90°$ for TQF spectra to eliminate other coherences (Bodenhausen et al. 1984; Jaccard et al. 1986; Pekar and Leigh 1986). Therefore, the contribution of the even-rank tensor is detected only by double-quantum filtering. Moreover, when $\theta = 54.7°$, the contribution of the T_{21} is detected exclusively (Chung and Wimperis 1990; Eliav et al. 1992; Jaccard et al. 1986; Shinar et al. 1993). The value of τ, the multiple-quantum creation or preparation time, varied between 0.005 and 100 ms; the evolution time, δ, was fixed at 10 μs. The other NMR parameters used for the ^{23}Na MQF NMR experiments were as follows: spectral width of 3 kHz, recycling time of 250 ms (TQF) or 600 ms ($DQF_{54.7}$), acquisition time of 200 ms (TQF) or 500 ms ($DQF_{54.7}$) and line broadening for signal-to-noise enhancement of 20 Hz.

Data analysis and processing

SQ intra- and extracellular ^{23}Na or ^{7}Li NMR signal integrals, A_i and A_e respectively, were quantitated using the standard Varian or Bruker software, and MQF signal quantitation was performed by a magnitude calculation after Fourier transformation, followed by point-to-point integration of the resultant peaks between user-defined break points. The intra- and extracellular Na^{+} and Li^{+} concentrations were determined according to a literature method (Gupta and Gupta 1982), using Eq. 2, taking into account the cytocrit (C_T), i.e., the total percentage volume of cells in the sample (for cells in general; for RBCs the hematocrit, Ht, is usually used) and the ratio of volume of intracellular water accessible to Li^{+} ions to cell volume (α):

$$[Li^{+}]_{if} = [Li^{+}]_{eT} \times \frac{A_i}{A_e} \times \frac{1 - C_T}{\alpha \times C_T} \quad (2)$$

where $[Li^{+}]_{if}$ is the free NMR visible intracellular Li^{+} concentration (in mmol (L cells)$^{-1}$, where the cell volume was evaluated from the cytocrit) and $[Li^{+}]_{eT}$ is the total Li^{+} concentration added to the sample; A_i and A_e are the areas of the intra- and extracellular ^{7}Li NMR resonances, respectively, taken at different times.

Li^+ influx rate constants (k_i) and the steady-state percentage of intracellular ^7Li resonance areas relative to the total area of intra- and extracellular ^7Li NMR resonances $[A_i/(A_i + A_e) \times 100]$ were calculated by fitting the data points using Eq. 3, which defines the first-order kinetics of Li^+ influx

$$\frac{(A_i)_t}{(A_i + A_e)_t} = \frac{(A_i)_\infty}{(A_i + A_e)_\infty} \times (1 - e^{-k_i t}) \quad (3)$$

where $(A_i)_t$, $(A_e)_t$ and $(A_i)_\infty$, $(A_e)_\infty$ are the areas of the intra- and extracellular $^7Li^+$ NMR signals at the different times t and when the intracellular Li^+ concentration has reached a steady state, respectively. The influx parameters were obtained by non-linear least squares fitting of the experimental data to the monoexponential function of Eq. 3 using the Origin™ 6.0 program (Microcal™ Software, Inc., USA).

The modulation of the isotropic T_{31} component intensity of the TQF signal by the τ values is given by Eq. 4 (Eliav et al. 1992):

$$S(\omega, \tau) = A \times \left[e^{-\frac{\tau}{T_{2s}}} - e^{-\frac{\tau}{T_{2f}}} \times \cos(\overline{\omega}_Q \tau) \right] \quad (4)$$

while the modulation of the absolute value of the anisotropic T_{21} of the $DQF_{54.7}$ signal intensity was fitted using Eq. 5 (Eliav et al. 1992):

$$S(\omega, \tau) = B \times e^{-\frac{\tau}{T_{2f}}} \times \sin(\overline{\omega}_Q \tau) \quad (5)$$

The values of the residual quadrupolar coupling constant ($\overline{\omega}_Q$), A and B constants (which represent the amplitudes of the T_{31} and T_{21} signals, respectively), T_{2f} and T_{2s} (fast and slow components, respectively, of the biexponential T_2 relaxation time) were obtained by fitting the TQF or $DQF_{54.7}$ signal areas *versus* the τ value data to the appropriate function in Eqs. 4 or 5 using the Origin™ 6.0 program (Microcal™ Software, Inc., USA), which employs a Marquart-Levenberg non-linear optimisation algorithm. In a first step of the analysis, the parameters in Eqs. 4 and 5 were allowed to vary simultaneously. After that, and in order to fine-tune the fitting procedure, $\overline{\omega}_Q$ was set to the best value(s) obtained in the previous optimisation step, and the data points were re-fitted by allowing the other parameters to vary. The goodness of the nonlinear regressions was evaluated by the corresponding R^2 values.

Acknowledgments The authors acknowledge financial support from Fundação para a Ciência e a Tecnologia (FCT), Portugal (Projects POCTI/2000/BCI/36160, PRAXIS/2/2.1/BIO/1117/95) and FEDER. Carla P. Fonseca, Liliana P. Montezinho, Luís L. Fonseca and Paula M. Alves were supported by FCT grants, Praxis XXI/BD/21462/99, SFRH/BD/3286/2000, PRAXIS XXI/BD/21532/99 and PRAXIS XXI/BD/2721/94, respectively. The assistance of Dr. Antonio Maretzek in setting up some of the NMR experiments is gratefully acknowledged.

References

Ahuja AS, Prasad KN, Hendee WR, Carson PL (1978) Thermal conductivity and diffusivity of neuroblastoma tumor. Med Phys 5:418–421

Alves PM, Flogel U, Brand A, Leibfritz D, Carrondo MJ, Santos H, Sonnewald U (1996) Immobilization of primary astrocytes and neurons for online monitoring of biochemical processes by NMR. Dev Neurosci 18:478–483

Bodenhausen G, Kogler H, Ernst RR (1984) Selection of coherence-transfer pathways in NMR pulse experiments. J Magn Reson 58:370–388

Borthakur A, Shapiro EM, Beers J, Kudchodkar S, Kneeland JB, Reddy R (2002) Effect of IL-1β-induced macromolecular depletion on residual quadrupolar interaction in articular cartilage. J Magn Reson Imaging 15:315–323

Brand A, Richter-Landsberg C, Leibfritz D (1997) Metabolism of acetate in rat brain neurons, astrocytes and cocultures: metabolic interactions between neurons and glia cells, monitored by NMR spectroscopy. Cell Mol Biol (Noisy-le-grand) 43:645–657

Brocklehurst KW, Pollard HB, Siddle K, Hutton J (1990) Peptide hormones: a practical approach. IRL Press Oxford

Chung CW, Wimperis S (1990) Optimum detection of spin -3/2 biexponential relaxation using multiple-quantum filtration techniques. J Magn Reson 88:440–447

Daly PF, Lyon RC, Straka EJ, Cohen JS (1988) ^{31}P-NMR spectroscopy of human cancer cells proliferating in a basement membrane gel. FASEB J 2:2596–2604

Dizon JM, Tauskela JS, Wise D, Burkhoff D, Cannon PJ, Katz J (1996) Evaluation of triple-quantum-filtered ^{23}Na NMR in monitoring of intracellular Na content in the perfused rat heart: comparison of intra- and extracellular transverse relaxation and spectral amplitudes. Magn Reson Med 35:336–345

Duvvuri U, Kaufman JH, Patel SD, Bolinger L, Kneeland JB, Leigh JS, Reddy R (1998) Sodium multiple quantum spectroscopy of articular cartilage: effects of mechanical compression. Magn Reson Med 40:370–375

Duvvuri U, Leigh JS, Reddy R (1999) Detection of residual quadrupolar interaction in the human breast in vivo using sodium-23 multiple quantum spectroscopy. J Magn Reson Imaging 9:391–394

Eliav U, Navon G (1994) Analysis of double-quantum-filtered NMR spectra of ^{23}Na in biological tissues. J Magn Reson B 103:19–29

Eliav U, Shinar H, Navon G (1992) The formation of a second-rank tensor in ^{23}Na double-quantum-filtered NMR as an indicator for order in a biological tissue. J Magn Reson 98:223–229

Flogel U, Willker W, Leibfritz D (1994) Regulation of intracellular pH in neuronal and glial tumour cells, studied by multinuclear NMR spectroscopy. NMR Biomed 7:157–166

Fonseca CP, Montezinho LP, Nabais C, Freitas H, Geraldes CFGC, Castro MMCA (2004) Effects of Li^+ transport and intracellular binding on Li^+/Mg^{2+} competition in bovine chromaffin cells. Biochim Biophys Acta 1691:79–90

Fujimoto T, Lee K, Miwa S, Ogawa K (1991) Immunocytochemical localization of fodrin and ankyrin in bovine chromaffin cells in vitro. J Histochem Cytochem 39:1485–1493

Gary-Bobo CM, Solomon AK (1968) Properties of hemoglobin solutions in red cells. J Gen Physiol 52:825–853

Grieve SM, Wickstead B, Torres AM, Styles P, Wimperis S, Kuchel PW (1998) Multiple-quantum filtered ^{17}O and ^{23}Na NMR analysis of mitochondrial suspensions. Biophys Chem 73:137–143

Gullapalli RP, Hawk RM, Komoroski RA (1991) A ^7Li NMR study of visibility, spin relaxation, and transport in normal human erythrocytes. Magn Reson Med 20:240–252

Gullapalli RP, Hawk RM, Komoroski RA (1992) Effect of lithium on the double-quantum behavior of ^{23}Na in normal human erythrocytes. Magn Reson Med 27:1–12

Gupta RK, Gupta P (1982) Direct observation of resolved resonances from intra- and extracellular ^{23}Na ions in NMR studies of intact cells and tissues using dysprosium(III)tripolyphosphate as paramagnetic shift reagent. J Magn Reson 47:344–350

Hancu I, van der Maarel C Jr, Boada FE (2002) Detection of sodium ions in anisotropic environments through spin-lock NMR. Magn Reson Med 47:68–74

Hays RM, Franki N, Simon H, Gao Y (1994) Antidiuretic hormone and exocytosis: lessons from neurosecretion. Am J Physiol 267:C1507–C1524

Hubbard PS (1970) Non exponential nuclear magnetic relaxation by quadrupolar interactions. J Chem Phys 53:985–987

Hutchison RB, Huntley JJ, Zhou HZ, Ciesla DJ, Shapiro JI (1993) Changes in double quantum filtered sodium intensity during prolonged ischemia in the isolated perfused heart. Magn Reson Med 29:391–395

Insko EK, Kaufman JH, Leigh JS, Reddy R (1999) Sodium NMR evaluation of articular cartilage degradation. Magn Reson Med 41:30–34

Jaccard G, Wimperis S, Bodenhausen G (1986) Multiple-quantum NMR spectroscopy of $S = 3/2$ spins in isotropic phase: A new probe for multiexponential relaxation. J Chem Phys 85: 6282–6293

Jelicks LA, Gupta RK (1989a) Double-quantum NMR sodium ions in cells and tissues. Paramagnetic quenching of extracellular coherence. J Magn Reson 81:586–592

Jelicks LA, Gupta RK (1989b) Observation of intracellular sodium ions by double-quantum-filtered ^{23}Na NMR with paramagnetic quenching of extracellular coherence by gadolinium tripolyphosphate. J Magn Reson 83:146–151

Jelicks LA, Gupta RK (1993) On the extracellular contribution to multiple quantum filtered ^{23}Na NMR of perfused rat heart. Magn Reson Med 29:130–133

Kalyanapuram R, Seshan V, Bansal N (1998) Three-dimensional triple-quantum-filtered ^{23}Na imaging of the dog head in vivo. J Magn Reson Imaging 8:1182–1189

Kemp-Harper R, Brown SP, Hughes CE, Styles P, Wimperis S (1997) ^{23}Na NMR methods for selective observation of sodium ions in ordered environments. Prog Nucl Magn Reson Spectrosc 30:157–181

Kemp-Harper R, Brown SP, Styles P, Wimperis S (1994) In vivo NMR of sodium ions in ordered environments. J Magn Reson B 105:199–203

Kirk K, Kuchel PW, Labotka RJ (1988) Hypophosphite ion as a ^{31}P nuclear magnetic resonance probe of membrane potential in erythrocyte suspensions. Biophys J 54:241–247

Knubovets T, Shinar H, Eliav U, Navon G (1996) A ^{23}Na multiple-quantum-filtered NMR study of the effect of the cytoskeleton conformation on the anisotropic motion of sodium ions in red blood cells. J Magn Reson B 110:16–25

Knubovets T, Shinar H, Navon G (1998) Quantification of the contribution of extracellular sodium to ^{23}Na multiple-quantum-filtered NMR spectra of suspensions of human red blood cells. J Magn Reson 131:92–96

Kushnir T, Knubovets T, Itzchak Y, Eliav U, Sadeh M, Rapoport L, Kott E, Navon G (1997) In vivo ^{23}Na NMR studies of myotonic dystrophy. Magn Reson Med 37:192–196

Langley OK, Perrin D, Aunis D (1986) α-Fodrin in the adrenal gland: localization by immunoelectron microscopy. J Histochem Cytochem 34:517–525

LaVerde G, Nemoto E, Jungreis CA, Tanase C, Boada FE (2007) Serial triple quantum sodium MRI during non-human primate focal brain ischemia. Magn Reson Med 57:201–205

Layden BT, Abukhdeir AM, Williams N, Fonseca CP, Carroll L, Castro MMCA, Geraldes CFGC, Bryant FB, Mota de Freitas D (2003) Effects of Li^+ transport and Li^+ immobilisation on Li^+/Mg^{2+} competition in cells: implications for bipolar disorder. Biochem Pharmacol 66:1915–1924

Ling W, Jerschow A (2007) Relaxation-allowed nuclear magnetic resonance transitions by interference between the quadrupolar coupling and the paramagnetic interaction. J Chem Phys 126: 064502

Lyon RC, McLaughlin AC (1994) Double-quantum-filtered ^{23}Na NMR study of intracellular sodium in the perfused liver. Biophys J 67:369–376

Lyon RC, Pekar J, Moonen CT, McLaughlin AC (1991) Double-quantum surface-coil NMR studies of sodium and potassium in the rat brain. Magn Reson Med 18:80–92

McCarthy KD, de Vellis J (1980) Preparation of separate astroglial and oligodendroglial cell cultures from rat cerebral tissue. J Cell Biol 85:890–902

Montezinho LP, Fonseca CP, Geraldes CFGC, Castro MMCA (2002) Quantification and localization of intracellular free Mg^{2+} in bovine chromaffin cells. Metal Based Drugs 9:69–80

Mota de Freitas D, Rong Q, Geraldes CFGC (1992) Effect of hematocrit on the rate of lithium uptake in human erythrocyte suspensions. Lithium 3:281–285

Navon G, Shinar H, Eliav U, Seo Y (2001) Multiquantum filters and order in tissues. NMR Biomed 14:112–132

Navon G, Werrmann JG, Maron R, Cohen SM (1994) ^{31}P NMR and triple quantum filtered ^{23}Na NMR studies of the effects of inhibition of Na^+/H^+ exchange on intracellular sodium and pH in working and ischemic hearts. Magn Reson Med 32:556–564

Nikolakopoulos J, Zachariah C, Mota de Freitas D, Geraldes CFGC (1996) Comparison of the use of gel threads and microcarrier beads in Li^+ transport studies of human neuroblastoma SH-SY5Y cells. Inorg Chim Acta 251:201–205

Nikolakopoulos J, Zachariah C, Mota de Freitas D, Stubbs EB, Ramasamy R, Castro MMCA, Geraldes CFGC (1998) ^{7}Li nuclear magnetic resonance study for the determination of Li^+ properties in neuroblastoma SH-SY5Y cells. J Neurochem 71:1676–1684

Ooms KJ, Cannella M, Vega AJ, Marcolongo M, Polenova T (2008a) ^{23}Na TQF NMR imaging for the study of spinal disc tissue. J Magn Reson 195:112–115

Ooms KJ, Cannella M, Vega AJ, Marcolongo M, Polenova T (2008b) The application of ^{23}Na double-quantum-filter (DQF) NMR spectroscopy for the study of spinal disc degeneration. Magn Reson Med 60:246–252

Payne GS, Seymour AM, Styles P, Radda GK (1990) Multiple quantum filtered ^{23}Na NMR spectroscopy in the perfused heart. NMR Biomed 3:139–146

Pekar J, Leigh JS Jr (1986) Detection of biexponential relaxation in sodium-23 facilitated by double-quantum filtering. J Magn Reson 69:582–584

Ramasamy R, Castro MMCA, Mota de Freitas D, Geraldes CFGC (1992) Lanthanide complexes of aminophosphonates as shift reagents for ^{7}Li and ^{23}Na NMR studies in biological systems. Biochimie 74:777–783

Reddy R, Bolinger L, Shinnar M, Noyszewski E, Leigh JS (1995) Detection of residual quadrupolar interaction in human skeletal muscle and brain in vivo via multiple quantum filtered sodium NMR spectra. Magn Reson Med 33:134–139

Reddy R, Li S, Noyszewski EA, Kneeland JB, Leigh JS (1997) In vivo sodium multiple quantum spectroscopy of human articular cartilage. Magn Reson Med 38:207–214

Richter-Landsberg C (1988) Nerve growth factor-inducible, large external (NILE) glycoprotein in developing rat cerebral cells in culture. Cell Tissue Res 252:181–190

Richter-Landsberg C, Besser A (1994) Effects of organotins on rat brain astrocytes in culture. J Neurochem 63:2202–2209

Savitz D, Sidel VW, Solomon AK (1964) Osmotic properties of human red cells. J Gen Physiol 48:79–94

Schepkin VD, Choy IO, Budinger TF, Obayashi DY, Taylor SE, DeCampli WM, Amartur SC, Young JN (1998) Sodium TQF NMR and intracellular sodium in isolated crystalloid perfused rat heart. Magn Reson Med 39:557–563

Seo Y, Murakami M, Suzuki E, Kuki S, Nagayama K, Watari H (1990) NMR characteristics of intracellular K in the rat salivary gland: a ^{39}K NMR study using double-quantum filtering. Biochemistry 29:599–603

Seshan V, Sherry AD, Bansal N (1997) Evaluation of triple quantum-filtered ^{23}Na NMR spectroscopy in the in situ rat liver. Magn Reson Med 38:821–827

Shinar H, Eliav U, Knubovets T, Sharf Y, Navon G (1995) Measurement of order in connective tissues by multiple quantum filtered NMR spectroscopy of quadrupolar nuclei. Q Magn Reson Biol Med 2:73–77

Shinar H, Knubovets T, Eliav U, Navon G (1993) Sodium interaction with ordered structures in mammalian red blood cells detected by ^{23}Na double quantum NMR. Biophys J 64:1273–1279

Springer CS Jr (1987) Measurement of metal cation compartmentalization in tissue by high-resolution metal cation NMR. Annu Rev Biophys Biophys Chem 16:375–399

Srinivasan C, Minadeo N, Toon J, Graham D, Mota de Freitas D, Geraldes CFGC (1999) Competition between Na^+ and Li^+ for unsealed and cytoskeleton-depleted human red blood cell membrane: a ^{23}Na multiple quantum filtered and ^{7}Li NMR relaxation study. J Magn Reson 140:206–217

Tauskela JS, Dizon JM, Cannon PJ, Katz J (1995) Detection of an extracellular contribution from a second-rank tensor to the double-quantum-filtered ^{23}Na NMR spectrum in the isolated perfused rat heart. J Magn Reson B 108:165–169

Tauskela JS, Shoubridge EA (1993) Response of the ^{23}Na NMR double-quantum filtered signal to changes in Na^+ ion concentration in model biological solutions and human erythrocytes. Biochim Biophys Acta 1158:155–165

Winter PM, Bansal N (2001) Triple-quantum-filtered ^{23}Na NMR spectroscopy of subcutaneously implanted 9L gliosarcoma in the rat in the presence of $TmDOTP^{5-}$. J Magn Reson 152:70–78

Winter PM, Poptani H, Bansal N (2001) Effects of chemotherapy by 1,3-bis(2-chloroethyl)-1-nitrosourea on single-quantum- and triple-quantum-filtered ^{23}Na and ^{31}P nuclear magnetic resonance of the subcutaneously implanted 9L glioma. Cancer Res 61: 2002–2007